Journal of Power Sources 236 (2013) 138–144

Contents lists available at SciVerse ScienceDirect

Journal of Power Sources

journal homepage: www.elsevier.com/locate/jpowsour

In situ Raman study on the structural degradation of a graphite composite negative-electrode and the influence of the salt in the electrolyte solution

Hiroe Nakagawa [a], Yasuhiro Domi [a], Takayuki Doi [a,*], Manabu Ochida [a], Shigetaka Tsubouchi [a], Toshiro Yamanaka [a], Takeshi Abe [b], Zempachi Ogumi [a]

[a] Office of Society-Academia Collaboration for Innovation, Kyoto University, Gokasho, Uji, Kyoto 611-0011, Japan
[b] Graduate School of Engineering, Kyoto University, Nishikyo-ku, Kyoto 615-8510, Japan

HIGHLIGHTS

- Surface crystallinity of graphite lowers in a $LiPF_6$-based electrolyte during the initial charge.
- The structural disordering is greater than that in a $LiClO_4$-based electrolyte.
- The structural degradation should be accelerated by the use of a large quantity of an electrolyte.

ARTICLE INFO

Article history:
Received 14 December 2012
Received in revised form
15 February 2013
Accepted 20 February 2013
Available online 28 February 2013

Keywords:
Graphite
Electrolyte salt
Cell design
Raman spectroscopy
Lithium ion battery

ABSTRACT

Structural changes in the surface of graphite composite electrodes in the 1st charge/discharge cycle were studied by *ex situ* and *in situ* Raman spectroscopy. The influence of the salt in the electrolyte solution and the volume of this solution injected into electrochemical cells on the structural degradation of the graphite surface was investigated. The surface crystallinity of graphite was degraded in $LiPF_6$-based electrolyte solution with only a cycle of intercalation/de-intercalation reactions of Li^+, compared to that in a $LiClO_4$-based electrolyte. *In situ* Raman measurements revealed that structural disordering of the graphite surface should occur in an early stage of the initial intercalation reaction of Li^+ into graphite.

© 2013 Elsevier B.V. All rights reserved.

1. Introduction

The electrochemical intercalation and de-intercalation of Li^+ at graphite have been widely used for charge and discharge reactions of negative electrodes in lithium ion batteries. The electrochemical reactions need to be maintained with high reversibility over 1000 or more cycles for 10–15 years if lithium ion batteries are to be used in large-sized applications such as electric-powered vehicles and stationary battery energy storage systems. To improve the cyclability and durability of lithium ion batteries, we must understand, and suppress, the mechanism that causes the degradation of graphite electrodes. Several factors that should cause a fading of the discharge capacity have been reported in the literature, such as the exfoliation of graphite layers due to solvent co-intercalation [1,2], the electronic isolation of graphite particles [3], and an increase in interfacial resistance [4]. In addition, electrolyte solutions, including solvents, salts and additives, have been shown to affect the charge/discharge performance of graphite negative-electrodes; e.g., Li^+ cannot be intercalated into graphite in propylene carbonate (PC)-based electrolyte solutions due to the poor compatibility of graphite and PC [5], while highly reversible intercalation and de-intercalation reactions of Li^+ proceed in ethylene carbonate (EC)-based solutions [6]. In addition, the interfacial resistance between carbonaceous negative-electrodes and electrolyte solution has been reported to be small with the use of lithium perchlorate ($LiClO_4$) as a salt, compared to lithium hexafluorophosphate ($LiPF_6$) and lithium tetrafluoroborate ($LiBF_4$) [7].

Laser Raman spectroscopy can detect Raman scattering near an electrode surface, and therefore is useful for investigating the surface crystal structure of electrodes. Hexagonal graphite crystallizes in the D^4_{6h} space group, and has two doubly degenerate Raman active E_{2g} modes at 42 and 1581 cm^{-1} [8]. Our group previously

* Corresponding author. Tel.: +81 774384977; fax: +81 774384996.
E-mail address: doi@saci.kyoto-u.ac.jp (T. Doi).

0378-7753/$ – see front matter © 2013 Elsevier B.V. All rights reserved.
http://dx.doi.org/10.1016/j.jpowsour.2013.02.060

studied the variation of the E_{2g} line with the electrode potential by *in situ* Raman spectroscopy [9]. As a result, the spectral changes were closely associated with the phase transitions of Li–graphite intercalation compounds (GICs), and occurred reversibly during a charge and discharge cycle; the intensity and frequency of the E_{2g} lines at around 1580 cm^{-1} varied with the phase transition of Li–GICs. The electrode potential upon the electrochemical intercalation of Li^+ was found to be determined by the surface stage of the Li–GICs.

When graphite (a carbonaceous material) has imperfections in its crystal structure or a finite crystal size, additional lines appear at around 1330 (D band) and 1620 cm^{-1} (D′ band) in Raman spectra [10]. Kostecki et al. reported that the intensity of a disorder-induced line that peaked at about 1360 cm^{-1} increased after prolonged charge and discharge cycles [11], and suggested that graphite should undergo structural disordering. We previously used edge plane highly oriented pyrolytic graphite (HOPG) as a model graphite electrode, and investigated changes in the surface crystal structure during the first two potential cycles by electrochemical Raman spectroscopy [12]. As a result, the surface crystallinity of graphite significantly decreased with the intercalation and de-intercalation reactions of Li^+ in 1 mol dm^{-3} $LiClO_4$/EC + diethyl carbonate (DEC). This irreversible structural degradation was suppressed by the addition of film-forming additives of vinylene carbonate to the electrolyte.

$LiPF_6$ has been widely used as a salt for electrolyte solutions in commercially available lithium ion batteries. $LiPF_6$ is known to decompose upon exposure to trace amounts of water to produce HF, which should have a detrimental effect on battery performance [13,14]. In this study, structural changes in the surface of graphite composite electrodes in the initial charge/discharge cycle were investigated in $LiPF_6$-based electrolyte solution by *ex situ* and *in situ* Raman spectroscopy. The influence of the salt in the electrolyte solution on the structural degradation of the graphite surface is discussed by comparing the results to those obtained in $LiClO_4$-based electrolyte solution.

2. Experimental

Cu foil coated with a graphite composite was used as a working electrode. The composite consisted of 95 wt% synthetic graphite particles (MAG, Hitachi Chemicals), 2 wt% acetylene black (Denka black, Denki Kagaku Kogyo), and 3 wt% binders. The binders used were styrene-butadiene rubber (SBR, BM400, Zeon) and carboxymethyl cellulose (CMC, Cellogen, Dai-ichi Kogyo Seiyaku) (1:1 by weight). The thickness of the graphite composite was 0.07 mm, and the geometric electrode area was 12 mm × 12 mm or 15 mm × 15 mm. The electrolyte solution used was 1 mol dm^{-3} $LiClO_4$ or $LiPF_6$ dissolved in a mixture of EC and DEC (1:1 by volume). The water content in the solution was less than 20 ppm. All potentials in the text reflect V vs. Li/Li^+.

A graphite composite electrode, a polypropylene (PP) microporous membrane separator (Celgard #2500, Celgard), and a counter electrode of lithium foil were stacked in this order between two aluminum-laminated films. Three sides of the films were heat-sealed to make a pouch, into which was injected about 2 ml of electrolyte solution. Finally, the remaining side was sealed to obtain a pouch cell. The cell assembly was carried out in an Ar-filled glove box with a dew point below −80 °C. The electrochemical properties of the graphite electrode were investigated by two methods using a potentiostat/galvanostat (SP-300, Biologic); one was cyclic voltammetry (CV), and the other was constant-current/constant-voltage (CCCV) charging and constant-current (CC) discharging. CV was performed for three cycles at a scan rate of 0.5 mV s^{-1} between 3.0 and 0.01 V. CCCV charging and CC discharging were also performed for three cycles. CCCV charging was carried out from 3.0 V to 0.01 V at a constant current rate so that a charge process should theoretically be completed in 10 h, i.e., a current rate of 0.1 C mA, followed by charging at a constant voltage of 0.01 V for 15 h. CC discharging was then conducted at a current rate of 0.1 C mA from 0.01 to 3.0 V. After the electrochemical measurements, the cell was transferred back to the glove-box, and disassembled for removal of the graphite composite electrode, which was rinsed with dimethyl carbonate (DMC), and then dried under vacuum at room temperature over 5 min. The electrode was sealed in an airtight PP/nylon bag for *ex situ* Raman measurement. Raman spectra were excited with the 632.81 nm line (50 mW) of a He–Ne laser. A 100-power objective lens was used to focus the excitation laser on the surface of the graphite electrode through the PP/nylon film. The scattered light was collected in a backscattering (180°) geometry. The Raman spectra were recorded using a spectrometer (HR-800, Horiba Jobin-Yvon) equipped with a multichannel charge coupled device (CCD) detector. The exposure time was 10 s and the scattering spectrum was integrated 3 times.

Changes in the surface structure of graphite composite electrodes were observed by *in situ* Raman spectroscopy. The electrochemical Raman cell used had an airtight structure, and was equipped with optically flat Pyrex® glass [15]. The graphite composite electrode was clipped between two SUS304 sheets with a hollow square with the minimum pressure required for holding it, and used as a working electrode. The electrode was irradiated with a laser beam through the Pyrex® glass to obtain Raman spectra. The distance between the surface of the electrode and the Pyrex® glass was minimized at about 1 mm to suppress scattering from electrolytes. Li foil was used as the reference and counter electrodes. The electrochemical Raman cell held about 50 ml of electrolyte solution. The electrochemical cell was assembled in an Ar-filled glove box. Electrochemical Li^+ intercalation (charge) and de-intercalation (discharge) at the graphite were carried out by changing the potential using SP-300; the electrode was swept from the open circuit potential (OCP) to 1.0 V at 0.5 mV s^{-1}, then from 1.0 to 0.1 V at 0.2 mV s^{-1}, and finally from 0.1 to 0.01 V at 0.1 mV s^{-1}. After the electrode was held at 0.01 V for 5 h, the potential was swept in an anodic direction up to 3.0 V, and kept at that potential for 5 h. Raman measurements were carried out continuously under potential control. The integration time for each measurement was 90 s, which is very short compared to the total charging and discharging time, and hence the spectral changes during each Raman measurement are considered to be negligible. Raman spectra were excited with the 632.81 nm line (50 mW) of a He–Ne laser through an objective lens: 10-power and 100-power long-focus objective lenses were used during potential control, and before and after potential cycling, respectively.

All experiments were carried out at an ambient temperature of ca. 25 °C.

3. Results and discussion

Fig. 1a shows cyclic voltammograms of a graphite composite electrode obtained in 1 mol dm^{-3} $LiClO_4$/EC + DEC. In the 1st cathodic scan, a cathodic current was present at potentials below about 1.8 V, and increased with a decrease in the electrode potential. The cathodic current in a potential range from about 1.8 to 0.7 V decreased after the 2nd cycle, as shown in the inset in Fig. 1a, and therefore the decrease in the cathodic current should be attributed to reductive decomposition of the electrolyte solution and the formation of surface films on graphite. An anodic current due to the de-intercalation of Li^+ from graphite was observed at around 0.4 V. A new cathodic current peak appeared at about 0.2 V in the 2nd cycle, and further increased in the 3rd cycle, suggesting that the stage

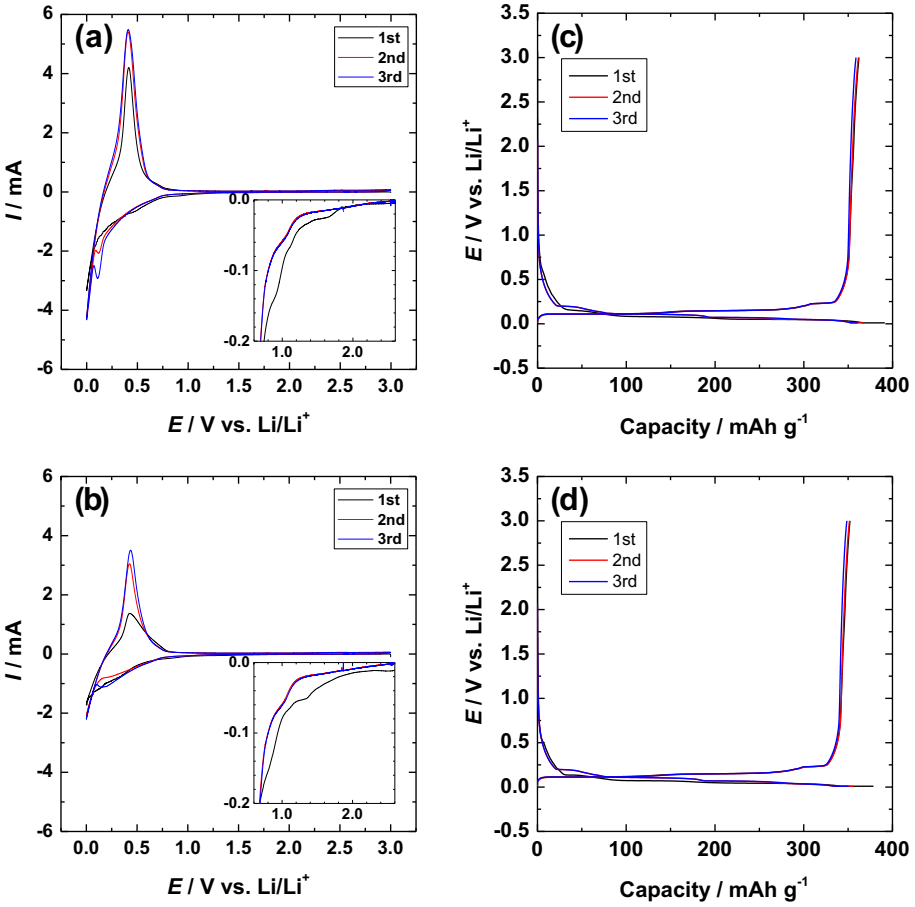

Fig. 1. (a, b) Cyclic voltammograms, and (c, d) charge and discharge curves of graphite composite electrodes between 3.0 and 0.01 V in (a, c) 1 mol dm^{-3} $LiClO_4$/EC + DEC (1:1 by volume) and (b, d) 1 mol dm^{-3} $LiPF_6$/EC + DEC (1:1 by volume). The scan rate was 0.5 mV s^{-1}. The charge and discharge currents were 0.1 C mA. The geometric electrode area was 12 mm × 12 mm. Each expansion of the 1st–3rd cycles between 0.6 and 2.6 V is shown in the inset in (a) and (b).

transformation of Li–GICs should be facilitated with repeated potential cycling. Fig. 1b shows cyclic voltammograms of a graphite composite electrode in 1 mol dm^{-3} $LiPF_6$/EC + DEC. A cathodic current became noticeable at potentials below about 2.0 V during the 1st potential cycle. The cathodic current in a potential range from about 2.0 to 0.7 V decreased after the 2nd cycle. Hence, this decrease should be attributed to reductive decomposition of the electrolyte solution and the formation of surface films. The irreversible cathodic current in the 1st cycle was different from that obtained in $LiClO_4$-based electrolyte solution; e.g., a shoulder peak was seen at around 1.7 and 1.4 V for $LiClO_4$- and $LiPF_6$-based electrolyte solutions, respectively. These differences indicate that the reductive decomposition reaction of the electrolyte solution and the formation reaction of surface films are not the same for these electrolytes. The Coulombic efficiency in the 1st cycle, which was estimated from the area of the redox currents, was 73% and 61% for $LiClO_4$- and $LiPF_6$-based electrolytes, respectively. These results suggest that surface films, i.e., solid state interphase (SEI), are more effectively formed in a $LiClO_4$-based electrolyte than in a $LiPF_6$-based electrolyte. The reversible redox currents, i.e., cathodic currents at 0 V and anodic current peaks at about 0.4 V, were larger for a $LiClO_4$-based electrolyte than for a $LiPF_6$-based electrolyte. In addition, the peak potential of the anodic currents was lower for a $LiClO_4$-based electrolyte (about 0.415 V) than for a $LiPF_6$-based electrolyte (about 0.430 V), which indicates greater polarization in a $LiPF_6$-based electrolyte. These results suggest that the intercalation and deintercalation reactions of Li^+ in a $LiClO_4$-based electrolyte should be more rapid than those in a $LiPF_6$-based electrolyte, while the ionic conductivity in 1 mol dm^{-3} $LiPF_6$/EC + DEC is greater than that in 1 mol dm^{-3} $LiClO_4$/EC + DEC [16,17].

Fig. 1c and d shows charge and discharge curves of graphite composite electrodes obtained in a mixture of EC and DEC containing 1 mol dm^{-3} $LiClO_4$ and $LiPF_6$, respectively. The charge and discharge capacities in the $LiClO_4$-based electrolyte in the 1st cycle were evaluated to be 391 and 362 mAh g^{-1}, respectively (Fig. 1c). The charge capacity exceeded the theoretical capacity of 372 mAh g^{-1}, and hence the irreversible capacity should be attributed to reductive decomposition of the electrolyte solution and the formation of surface films. On the other hand, in the $LiPF_6$-based electrolyte, the charge and discharge capacities in the 1st cycle were 379 and 352 mAh g^{-1}, respectively (Fig. 1d). The discharge/charge efficiency was evaluated to be about 93%, which was the same as that obtained for the $LiClO_4$-based electrolyte (93%). In the 2nd cycle, the charge and discharge capacities decreased to 356 and 352 mAh g^{-1} in the $LiPF_6$-based electrolyte solution, respectively. In the $LiClO_4$-based electrolyte, the charge and discharge capacities also decreased to 367 and 362 mAh g^{-1} in the 2nd cycle, respectively. The discharge/charge efficiency reached about 99% in both cases, which suggests that further decomposition of the electrolyte solution was suppressed after the 2nd cycle by the formation of superior surface films during the 1st cycle. The charge capacities consisted of those charged in CC (3.0 V–0.01 V)- and CV (0.01 V)-modes; the former in the 2nd cycle was evaluated to be 353 and 333 mAh g^{-1} in $LiClO_4$- and $LiPF_6$-based electrolyte solutions, respectively. The latter was 14 and 23 mAh g^{-1} in $LiClO_4$- and $LiPF_6$-based electrolytes, respectively. Thus, the capacity charged in

CC-mode for the $LiClO_4$-based electrolyte was greater than that obtained for the $LiPF_6$-based electrolyte. These results suggest that the intercalation reaction of Li^+ at graphite should be more rapid in the $LiClO_4$-based electrolyte than in the $LiPF_6$-based electrolyte solution, which is in good agreement with the cyclic voltammograms shown in Fig. 1a and b.

Fig. 2a and b shows *in situ* Raman spectra of graphite composite electrodes obtained during the initial cathodic scan from OCP to 0.01 V in EC + DEC containing 1 mol dm^{-3} $LiClO_4$ and $LiPF_6$, respectively. A line that peaks at 1580 cm^{-1} was observed before potential cycling in both $LiClO_4$ (3.234 V)- and $LiPF_6$ (3.558 V)-based electrolyte solution. This line is well known to be related to the crystallinity of carbonaceous materials, and is assigned to the Raman active E_{2g} mode frequency (G band) [18]. The other observed lines were assigned to Raman scattering from solvents and salts in the electrolytes [16,19].

Variation of the Raman shift of the lines at around 1580 cm^{-1} (symbols on the tertiary vertical axis on the right edge), the electrode potential (black line on the vertical axis on the left), the current (blue dotted line on the primary vertical axis on the right), and the integrated charge amount in the 1st cycle in EC + DEC containing 1 mol dm^{-3} $LiClO_4$ and $LiPF_6$ (green dashed line on the secondary vertical axis on the right) are summarized in Fig. 3a and b, respectively. When the electrode potential was scanned from OCP to 0.01 V in 1 mol dm^{-3} $LiClO_4$/EC + DEC, the G band gradually shifted from around 1580 cm^{-1} toward higher wavenumbers at potentials below about 1.0 V where the cathodic current began to flow, and reached about 1590 cm^{-1} at around 0.2 V, as shown in Fig. 3a. In this potential region, no lines indicative of staged phases were observed, indicating that Li^+ was intercalated randomly between every layer of graphite; i.e., a dilute stage-1 phase was formed [9]. Two new lines appeared at about 1575 and 1600 cm^{-1} on both sides of the original line when the electrode potential reached about 0.2 V. The intensity of the new lines increased with time, while that of the original line decreased. Based on the literature, the new lines were assigned to the interior and bounding layer modes of stage-4, i.e., a phase transition from dilute stage-1 to stage-4 occurred [9]. These two lines formed a broad peak at around 1580 cm^{-1} when the electrode potential was held at 0.01 V, and then gradually disappeared. This behavior indicates that phase transitions from stage-4 through stages-3 and -2 to stage-1 occurred [9]. When the electrode potential was swept in an anodic direction from 0.01 V, two lines assigned to stage-4 appeared again at about 1575 and 1600 cm^{-1} at around 0.6 V. These two lines became a single line at about 1590 cm^{-1} at about 0.8 V, and gradually shifted to lower wavenumbers. A sharp peak finally returned at the original position of 1580 cm^{-1}. These results clearly indicate that the phase transitions of Li–GICs proceeded almost reversibly during a potential cycle between 3 and 0.01 V [5].

When the electrode potential was swept from OCP to 0.01 V in 1 mol dm^{-3} $LiPF_6$/EC + DEC, a line assigned to the G band gradually shifted from 1580 to 1590 cm^{-1} at potentials below about 1.0 V,

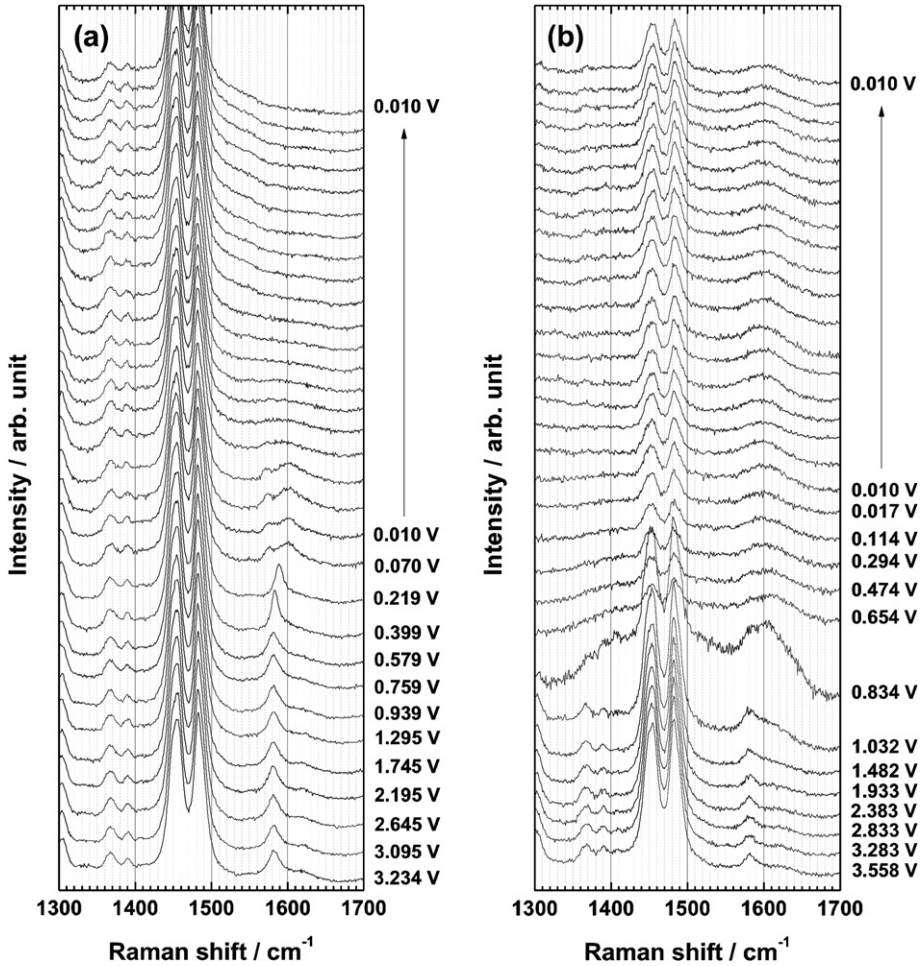

Fig. 2. *In situ* Raman spectra of graphite composite electrodes obtained at potentials ranging from 3.0 to 0.01 V during the initial cathodic polarization in (a) 1 mol dm^{-3} $LiClO_4$/EC + DEC (1:1 by volume) or (b) 1 mol dm^{-3} $LiPF_6$/EC + DEC (1:1 by volume).

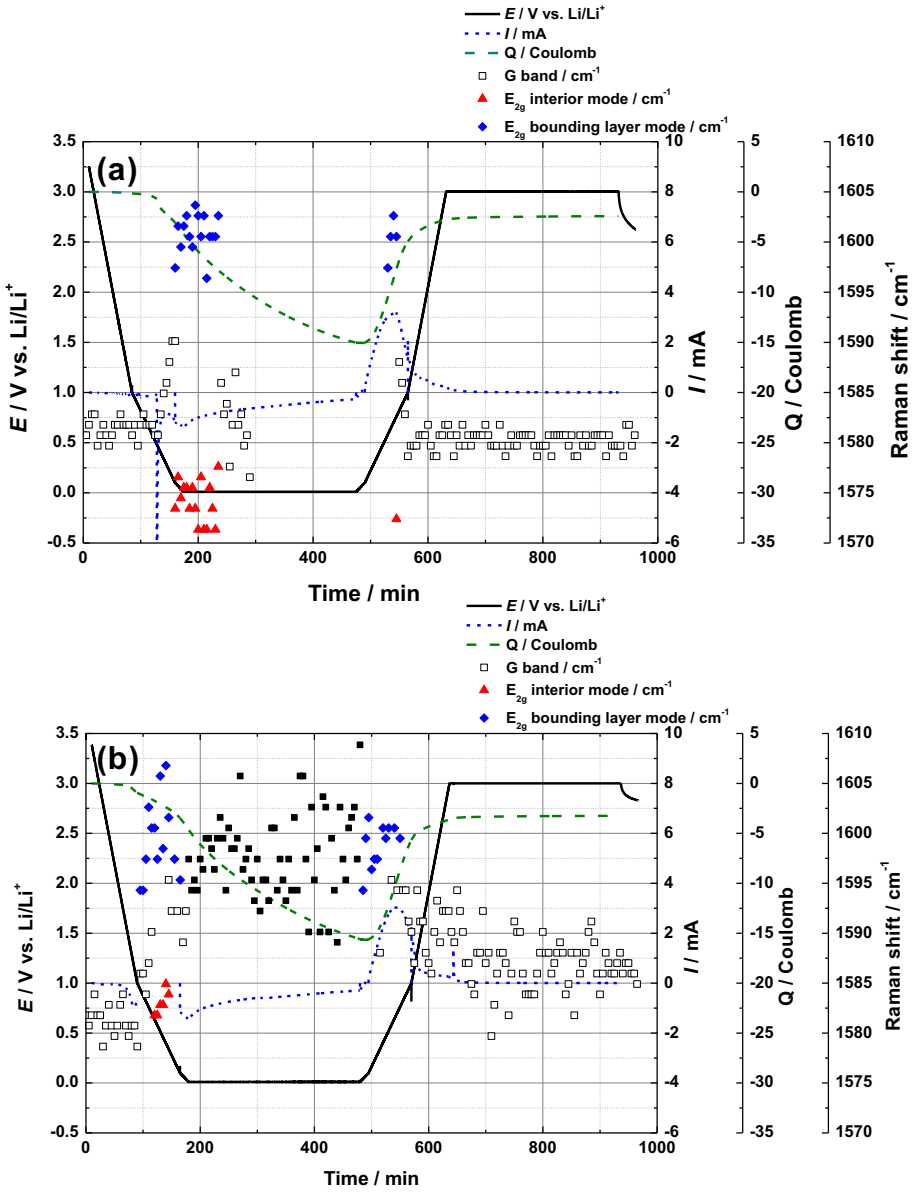

Fig. 3. Variation of the electrode potentials of graphite composite electrodes (black line on the vertical axis on the left), current (blue dotted line on the primary axis on the right), integrated charge amount (green dashed line on the secondary axis on the right), and Raman shift of the lines at around 1580 cm^{-1} (□, ▲, ◆ on the tertiary axis on the right edge) with time in the 1st potential cycle between 3.0 and 0.01 V in (a) 1 mol dm^{-3} $LiClO_4$/EC + DEC (1:1 by volume) or (b) 1 mol dm^{-3} $LiPF_6$/EC + DEC (1:1 by volume). The geometric electrode area was 12 mm × 12 mm. (For interpretation of the references to color in this figure legend, the reader is referred to the web version of this article.)

followed by the appearance of new two lines at around 1580 and 1600 cm^{-1} at about 0.6 V (Fig. 3b). This behavior was similar to that obtained in $LiClO_4$-based electrolyte solution. However, after the two lines became a single peak at about 0.01 V, it remained at around 1595–1600 cm^{-1} even while the potential was held at 0.01 V, as indicated by the closed square in Fig. 3b. When the potential was swept in an anodic direction from 0.01 V, the peak gradually shifted to lower wavenumbers, and finally reached about 1585 cm^{-1} at 3.0 V; it still remained broad and never returned to the original position of 1580 cm^{-1}. These results indicate that the phase transitions of Li–GICs should proceed irreversibly in $LiPF_6$-based electrolyte solution, unlike in $LiClO_4$-based electrolyte. The structural disordering of the graphite surface should occur in an early stage of the initial intercalation reaction of Li^+ into graphite where a peak appeared at around 1595–1600 cm^{-1}.

Fig. 4 shows *in situ* Raman spectra of the graphite composite electrodes before and after a potential cycle. These spectra were obtained through a 100-power long-focus objective lens to suppress Raman scattering from the Pyrex® glass and the electrolyte solution in the electrochemical Raman cell. Each spectrum showed several peaks related to graphite, i.e., a G band at around 1580 cm^{-1} and two peaks at around 1330 and 1620 cm^{-1}. The peak at around 1330 cm^{-1} is ascribed to the Raman inactive A_{1g} mode frequency [10]. The peaks at around 1330 (D band) and 1620 cm^{-1} (D′ band) appear in the case of a finite crystal size and imperfections in the carbonaceous materials [10]. The other lines observed in Fig. 4 were assigned to Raman scattering from solvents and salts in the electrolytes [16,19]. No obvious change in Raman spectra was observed before and after potential cycling in 1 mol dm^{-3} $LiClO_4$/EC + DEC, as shown in Fig. 4a and b. On the other hand, the peak intensities of

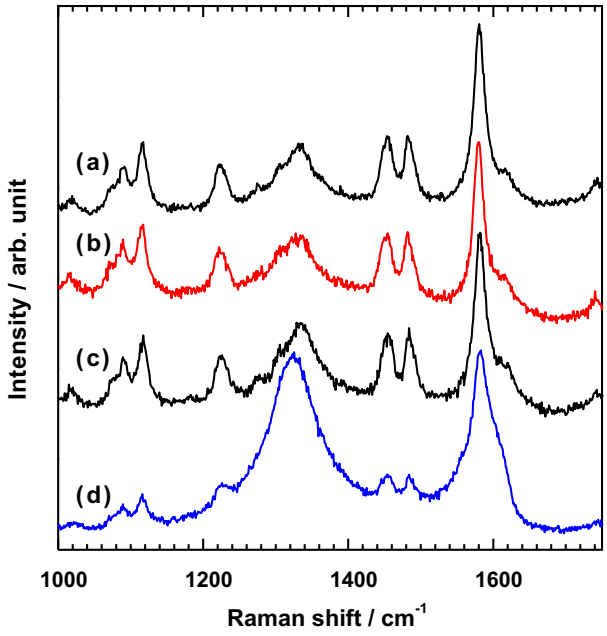

Fig. 4. Raman spectra of graphite composite electrodes (a, c) before and (b, d) after a potential cycle between 3.0 and 0.01 V with electrochemical Raman cells. The electrolyte solution used was (a, b) 1 mol dm^{-3} $LiClO_4$/EC + DEC (1:1 by volume) or (c, d) 1 mol dm^{-3} $LiPF_6$/EC + DEC (1:1 by volume).

the D and D′ bands remarkably increased in 1 mol dm^{-3} $LiPF_6$/EC + DEC, as shown in Fig. 4c and d. These results clearly indicate that the crystallinity of graphite should decrease during potential cycling in $LiPF_6$-based electrolyte solution [12].

Fig. 5a–c shows Raman spectra of graphite composite electrodes before and after CV in pouch cells using 1 mol dm^{-3} $LiPF_6$/EC + DEC and 1 mol dm^{-3} $LiClO_4$/EC + DEC. The peak intensities of the D and D′ bands increased after a potential cycle in $LiPF_6$-based electrolyte solution (Fig. 5c), compared to that obtained before potential cycling (Fig. 5a), whereas no obvious changes in the D and D′ bands were seen for the $LiClO_4$-based electrolyte (Fig. 5b). These results were very similar to those obtained in Fig. 4; the structural disordering of graphite in $LiPF_6$-based electrolyte solution was observed with the use of practical pouch cells, as is the case for the use of specially-designed electrochemical Raman cells (Fig. 4d). Fig. 5d and e shows Raman spectra of graphite composite electrodes after the 1st cycle of CCCV charging/CC discharging in pouch cells using 1 mol dm^{-3} $LiClO_4$/EC + DEC and $LiPF_6$/EC + DEC, respectively. D and D′ bands increased after charging/discharging specifically in $LiPF_6$-based electrolyte solution, as shown in Fig. 5e. Based on the above results, structural degradation of the graphite surface should occur regardless of the charge/discharge method, i.e., regardless of whether charging and discharging are performed under potential- or current-control.

The ratio of the intensity of the D band to that of the G band (I_D/I_G) serves as an index of the disordering of the crystal structure of the graphite surface. This value was evaluated from the Raman spectra of the graphite composite electrodes shown in Figs. 4 and 5, and the results are summarized in Fig. 6. In addition, a graphite composite electrode was charged and discharged in a pouch cell under the same conditions as those for *in situ* Raman measurement, and the values of I_D/I_G before and after potential cycling are shown by closed triangles in Fig. 6; i.e., a graphite composite electrode was swept in a pouch cell from OCP to 1.0 V at 0.5 mV s^{-1}, then from 1.0 to 0.1 V at 0.2 mV s^{-1}, and finally from 0.1 to 0.01 V at 0.1 mV s^{-1}. After the electrode was held at 0.01 V for 5 h, the potential was swept in an anodic direction up to 3.0 V, and kept at that potential for 5 h. The graphite electrode was then removed from the pouch cell to obtain a Raman spectrum. No significant change in I_D/I_G was observed for the $LiClO_4$-based electrolyte solution regardless of the type of electrochemical cell or the charge/discharge method, as indicated by red symbols. On the other hand, the value of I_D/I_G increased for the $LiPF_6$-based electrolyte solution, as shown by blue symbols. In particular, a considerable increase was observed after potential cycling using the laboratory-made electrochemical Raman cell, as indicated by blue closed circles. These results should be caused by a difference in cell design between the pouch cell and the electrochemical Raman cell because the increase in I_D/I_G was suppressed when a pouch cell was used, as indicated by blue closed

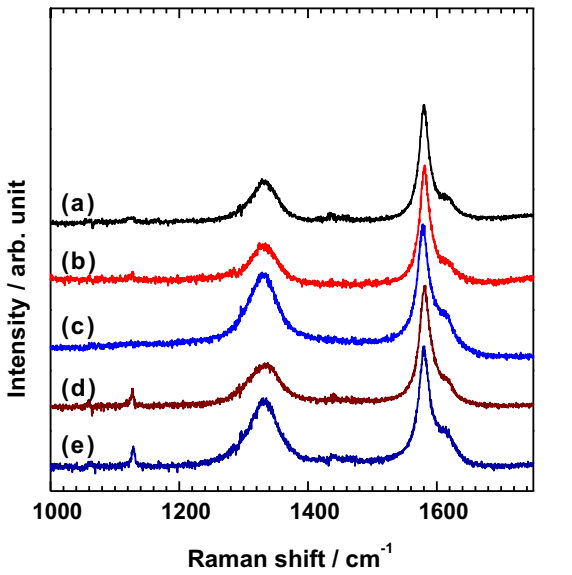

Fig. 5. Raman spectra of graphite composite electrodes (a) before and (b, c) after cyclic voltammetry, and (d, e) after CCCV charging and CC discharging with pouch cells. The electrolyte solution used was (b, d) 1 mol dm^{-3} $LiClO_4$/EC + DEC (1:1 by volume) or (c, e) 1 mol dm^{-3} $LiPF_6$/EC + DEC (1:1 by volume).

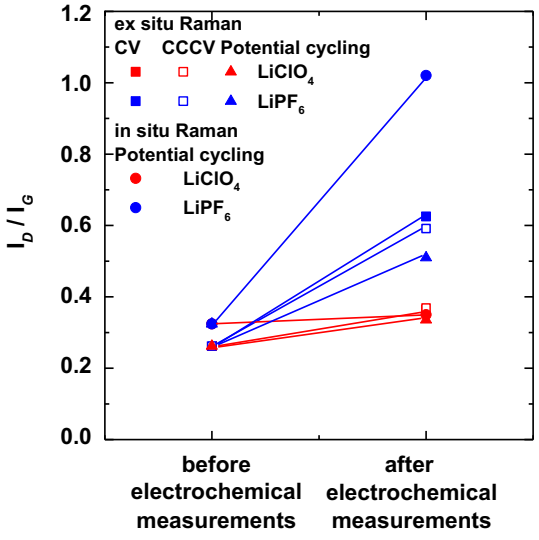

Fig. 6. I_D/I_G ratios of graphite composite electrodes before and after (●, ▲) potential cycling, (■) cyclic voltammetry, and (□) CCCV charging and CC discharging. The cells used were (●) electrochemical Raman cells and (■, □, ▲) pouch cells. The electrolyte solution used was 1 mol dm^{-3} $LiClO_4$/EC + DEC (1:1 by volume) or 1 mol dm^{-3} $LiPF_6$/EC + DEC (1:1 by volume).

triangles (in the web version); the geometric areas of the graphite composite electrodes used were 1.44 and 2.25 cm^2 for the pouch cell and electrochemical Raman cell used in this work. On the other hand, the pouch cell accommodated about 2 ml of electrolyte solution, while an excessive amount of electrolyte solution (about 50 ml) was used for the electrochemical Raman cell. Thus, the ratio of the amount of electrolyte solution to the electrode area was much higher for the electrochemical Raman cell than for the pouch cell. These facts suggest that the structural degradation of graphite should be accelerated by the use of a large quantity of electrolyte solution. In fact, the irreversible capacity in the 1st cycle for the electrochemical Raman cell (75 mAh g^{-1}) was much higher than that for the pouch cell (19 mAh g^{-1}). In addition, the Coulombic efficiency in the 1st cycle was much lower for the electrochemical Raman cell (80%) than for the pouch cell (95%). Thus, severe irreversible reactions occurred in the electrochemical Raman cell with a massive amount of electrolyte solution, which should be related to the structural deterioration of graphite.

4. Conclusion

In situ Raman measurements of graphite composite negative-electrodes revealed that structural degradation of a graphite surface should occur in an early stage of the initial intercalation reaction of Li^+ at graphite in 1 mol dm^{-3} $LiPF_6$/EC + DEC, whereas highly reversible intercalation/de-intercalation reactions of Li^+ proceeded in 1 mol dm^{-3} $LiClO_4$/EC + DEC. The D and D′ bands remarkably increased in Raman spectra after the initial charge/discharge cycle in 1 mol dm^{-3} $LiPF_6$/EC + DEC, and particularly when a specially-designed Raman cell with a large quantity of electrolyte solution was used, compared to the use of pouch cells. These results indicate that structural deterioration of the graphite surface in 1 mol dm^{-3} $LiPF_6$/EC + DEC should be accelerated when the ratio of the amount of electrolyte solution to the electrode area is high.

Acknowledgments

This work was supported by the New Energy and Industrial Technology Development Organization (NEDO) under contract from the Research & Development Initiative for Scientific Innovation of New Generation Batteries (RISING).

References

[1] J.O. Besenhard, H.P. Fritz, J. Electroanal. Chem. Interfacial Electrochem. 53 (1974) 329.
[2] M. Inaba, Z. Siroma, A. Funabiki, Z. Ogumi, Langmuir 12 (1996) 1535.
[3] D. Aurbach, M.D. Levi, E. Levi, A. Schechter, J. Phys. Chem. B 101 (1997) 2195.
[4] D. Aurbach, B. Markovsky, A. Rodkin, M. Cojocaru, E. Levi, H.-J. Kim, Electrochim. Acta 47 (2002) 1899.
[5] A.N. Dey, B.P. Sullivan, J. Electrochem. Soc. 117 (1970) 222.
[6] R. Fong, U. Sacken, J.R. Dahn, J. Electrochem. Soc. 137 (1990) 2009.
[7] D. Aurbach, Y. Ein-Eli, B. Markovsky, A. Zaban, S. Luski, Y. Carmeli, H. Yamin, J. Electrochem. Soc. 142 (1995) 2882.
[8] R.J. Nemanich, G. Lucovsky, S.A. Solin, Solid State Commun. 23 (1977) 117.
[9] M. Inaba, H. Yoshida, Z. Ogumi, T. Abe, Y. Mizutani, M. Asano, J. Electrochem. Soc. 142 (1995) 20.
[10] F. Tuinstra, J.L. Koenig, J. Chem. Phys. 53 (1970) 1126.
[11] R. Kostecki, F. McLarnon, J. Power Sources 119–121 (2003) 550.
[12] H. Nakagawa, Y. Domi, T. Doi, M. Ochida, S. Tsubouchi, T. Yamanaka, T. Abe, Z. Ogumi, J. Power Sources 206 (2012) 320.
[13] K. Tasaki, K. Kanda, S. Nakamura, M. Ue, J. Electrochem. Soc. 150 (2003) A1628.
[14] U. Heider, R. Oesten, M. Jungnitz, J. Power Sources 81–82 (1999) 119.
[15] M. Inaba, H. Yoshida, Z. Ogumi, J. Electrochem. Soc. 143 (1996) 2572.
[16] B. Klassen, R. Aroca, M. Nazri, G.A. Nazri, J. Phys. Chem. B 102 (1998) 4795.
[17] M. Morita, Y. Asai, N. Yoshimoto, M. Ishikawa, J. Chem. Soc. Faraday Trans. 94 (1998) 3451.
[18] R.J. Nemanich, S.A. Solin, Solid State Commun. 23 (1977) 417.
[19] F.S. Mortimer, Spectrochim. Acta 9 (1957) 270.